ELSEVIER

Journal of Nuclear Materials 273 (1999) 182–191

journal of nuclear materials

www.elsevier.nl/locate/jnucmat

Characterization of Zircaloy-4 oxide layers by impedance spectroscopy

P. Barberis [a,*], A. Frichet [b]

[a] *CEZUS, Center de Recherches, 73403 Ugine cedex, France*
[b] *FRAMATOME, 10 rue Juliette Récamier, 69456 Lyon cedex 06, France*

Received 21 September 1998; accepted 18 January 1999

Abstract

Two Zircaloy-4 type alloys with different tin contents (0.5 and 1.2 wt%) have been oxidized in autoclave (400°C in steam) for several durations (1–140 days). The film has been characterized by electrochemical impedance spectroscopy (EIS). Several soaking times have been investigated (up to 40 days). The Cole–Cole representation has been used to display and study the data. A simple electrical model has been derived from the observed spectra: the electrical circuit includes two RC loops in series, whose capacitances are frequency dispersed. It is thoroughly related to the layer structure. It has been shown that even before the kinetic transition, the film is constituted of three parts: an inner layer which is compact, an outer layer subdivided in an external region immediately soaked by the electrolyte, and an internal one in which electrolyte diffusion processes can take place. The kinetic transition is interpreted in terms of an abrupt 'compacity' change, both layers degrading at this point. The alloy with high tin content exhibits higher dispersive properties of the oxide layer formed on it, in correlation with its faster oxidation kinetics.

1. Introduction

The corrosion kinetics of Zircaloy-4 in high temperature high pressure steam or water can be schematically described [1] by a first parabolic-type regime, up to the so-called transition point, followed by a series of parabolic curves often approximated by a linear law. After longer times in the corroding environment, the kinetics increase sharply leading to the destruction of the sample (break away). The parabolic type laws are interpreted as a diffusion limiting transport of oxygen ions across a dense oxide layer [2], the deviation from the parabola being due either to stresses (Ref. [1], p. 46) or to grain size evolution [3]. At the transition point, the oxide layer looses its protective character, resulting in a more direct access of the steam to the metal surface, and an increase in corrosion rate. The linear corrosion rate can then be interpreted as the diffusion limited transport through a dense layer with an average constant thickness of about 2–3 μm [2].

Despite numerous works, little evidence has been obtained concerning the degradation of the oxide layer microstructure at the transition point. If cracks (generally parallel to the metal/oxide surface) appear around the transition, no pores going from the oxide surface to the metal have been detected by transmission electron microscopy. The morphology of the oxide crystallites does not evolve at the transition. Recent investigations by X-ray diffraction or Raman spectroscopy do not evidence any abrupt change in the crystallography of the oxide film, particularly the tetragonal to monoclinic ratio [4,5].

On another hand, electrochemical impedance spectroscopy (EIS) has been used since more than 30 years to characterize the oxide layer [6–17], particularly to determine the compact/porous nature of the film and the thickness of the compact layer [18–23]. In some cases, in situ measurements were performed during the corrosion [24,25].

However, no consensus is obtained on the results due of course to the wide variety of materials and corrosion

* Corresponding author. E-mail: barberis.crcezus@ugine savoie.usinor.com

0022-3115/99/$ – see front matter
PII: S0022-3115(99)00025-2

conditions studied by the different authors, but also to some difficulties specific to the EIS technique, that are summarized below:

- The measurements are made on a limited frequency range, in some cases at only one frequency, which is not sufficient to choose a model.
- The oxide film is essentially capacitive when it is thin (a few microns) and the impedance modulus reaches several MΩ or even GΩ at low frequencies (1 mHz), values difficult to measure.
- As a consequence of this capacitive behavior, Bode or Nyquist plots, generally used by authors do not display properly the characteristics of the spectra.
- The dielectric constant of the oxide film is not known accurately, and is assumed or computed between 13 and 22 or even more; this prevents any reliable determination of the overall oxide thickness.
- The impedance spectra are generally interpreted through 'equivalent electrical circuit', from the more simple (a capacity and a resistance in series [6]) to the more complex (see Ref. [13]), whose physical significance is unclear. In addition several fitting procedures can be used and leads to different results.
- Last, the capacitances used in the equivalent circuits have been recognized not to be ideal capacitances, but they exhibit a frequency dispersion. They are then modeled by constant phase elements (CPE) or Jonscher capacitance. The frequency dispersion parameters have no undoubtful physical meaning, and specially the CPE, if not associated in parallel with an ideal capacitance, leads to an impedance which equals zero at infinite frequency and infinite at zero frequency, which is troublesome.

In this work, we investigated two Zircaloy type materials with different tin contents, oxidized in autoclave. Impedance spectra were obtained after several soaking times of the sample in the electrolyte to investigate the porosity of the films. A careful analysis and fitting of the spectra, displayed in some convenient way, allowed us to propose a simple electrical equivalent circuit, and to study the transition point.

2. Experimental

2.1. Materials

Two Zircaloy-4 type alloys have been elaborated at a laboratory scale as 1 mm thick sheets. Their chemical compositions (Sn, Fe 0.2 wt%, Cr 0.1 wt%, O 0.12 wt%) were differing only by the tin content: 1.2 and 0.5 wt%. They will be called below Zy4-1.2% and Zy4-0.5%. They were in the recrystallized state, the last annealing being 1.5 h at 730°C, and the cumulative annealing parameter 2.10^{-17} h (see Ref. [4]).

Samples from the same Zy4-1.2% sheet were used in other corrosion related studies [4,5]. Samples of 20 × 30 mm were cut, degreased (alcohol/acetone) and etched (HF/HNO_3/water) prior to oxidation in a static autoclave in steam at 400°C, 10.5 MPa for up to 140 J.

2.2. Impedance measurements

Each sample was submitted to impedance measurements in H_2SO_4 0.1M at room temperature, the soaking by the electrolyte reaching about 40 days. The area investigated was 1 cm^2, delimited by a Teflon joint. The configuration used was a two-electrode, the counter-electrode being a Zircaloy-4 sheet. We checked that the impedance of the counter-electrode was negligible compared to that of the oxide film.

The frequency response analyzer was a Solartron 1253, allowing a frequency range from 20 kHz to 1 mHz to be investigated. A special impedance adaptator developed by the Pechiney Research Center in Voreppe (France) was used. It allows in particular to change automatically the calibration resistance from 1 Ω to 10 MΩ when the measured impedance modulus increases, to optimize the accuracy. With such a device, impedances up to 10 GΩ are accurately measured.

3. Methodology

3.1. Cole–Cole diagram

The impedance spectra have been displayed, besides the Bode and Nyquist plots, in the Cole–Cole diagram. It consists in considering the measured spectrum as due to a capacitance C^* in series with a resistor (here the resistance at infinite frequency, i.e. the electrolyte resistance) (Fig. 1). The evolution of the imaginary part C'' versus the real part C' of C with the frequency is the Cole–Cole diagram. This diagram is useful to study an essentially capacitive circuit, because it suppresses the large variation in $1/\omega$ of the impedance modulus with the frequency. It has been used previously by several authors, for example Jonscher (see his review report [26]), and applied to zirconium oxide film by Bataillon et al. [7].

On this diagram, we can extrapolate the high frequency data to infinite frequency: the intersection of the straight line with the C' axis gives the capacitance at infinite frequency C'_∞ directly related with the oxide layer thickness th by

$$C'_\infty = \frac{\varepsilon_o \varepsilon_r S}{\mathrm{th}} \tag{1}$$

with ε_o the vacuum permittivity, ε_r the relative permittivity and S the surface of the sample. This formula assumes that the interfaces are perfectly plane and parallel, and that the oxide layer is homogeneous.

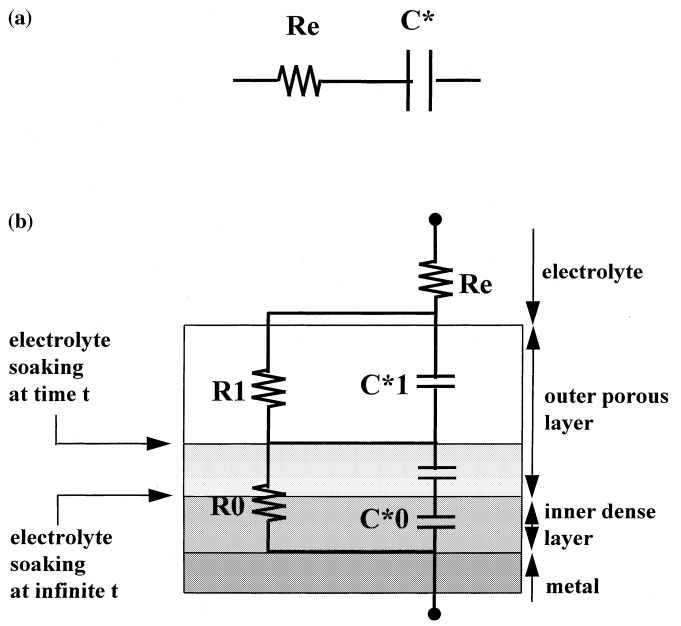

Fig. 1. Equivalent circuits used (a) to display the Cole–Cole diagram, (b) to model the oxide layer. Re represents the electrolyte resistance, C^* the equivalent complex capacitance, C_i^* the complex capacitances (frequency dispersed according to Jonscher's formula), R_i the resistances. The subscript 0 and 1 refer, respectively, to the inner and outer layer of the oxide film.

3.2. Dispersion factor

We define the dispersion factor for a given sample by

$$\mathrm{df}'(\omega) = \frac{C'(\omega) - C'_\infty}{C'_\infty} \tag{2}$$

with $C'(\omega)$ the real part of the capacitance, ω being the pulsation, i.e. $\omega = 2\pi f$, with f the frequency of the measurement. Though it can be defined at any measured frequency, we will compute it for the lowest one, i.e. a few mHz. This factor, not directly dependent on the thickness and independent on the chosen equivalent circuit and on the fitting, gives us a global indication of the frequency dispersion of the capacitance of the oxide layer, and will shed some light on the transition mechanism.

3.3. Equivalent circuit

The chosen electrical equivalent circuit is displayed in Fig. 1(b). It satisfies several requirements:

- to be simple,
- to have physical meaning, and
- to be compatible with all spectra, whatever the alloy, the oxidation and the soaking times.

The capacitances C_0^* and C_1^* are frequency dispersed according to Jonscher's formula [26]:

$$C_i^* = C_i^\infty \left(1 + \left(\frac{\omega_i}{j\omega}\right)^{1-n_i}\right), \tag{3}$$

where C_i^∞ is the capacitance at infinite frequency, ω_i the characteristic pulsation, and n_i the dispersion index (do not mistake with the dispersion factor). In the following, we will use the characteristic frequency f_i defined by $\omega_i = 2\pi f_i$ rather than the pulsation.

3.4. Physical meaning of the parameters

We will see below that:

- R_e represents the electrolyte resistance,
- C_0^∞ and C_1^∞ are related to the thickness of the inner and outer layers of the oxide,
- R_0 and R_1 are the corresponding resistances, and
- ω_0, ω_1 and n_0, n_1 the corresponding frequency dispersion parameters.

These last parameters have no evident physical interpretation. A few values of n have been theoretically computed, for example n equals 0.5 when diffusion processes are taken into account (Warburg impedance, see for example Ref. [27]), and some other values when modeling porous or fractal structures, or gradients. However, Jonscher's formula is quite universal, and will be used 'better lacking'.

3.5. Fitting procedure

A fitting computer program has been developed and described elsewhere [28]. It is based on both simulated annealing and non-linear least square procedure. The main difficulty is in fact to define the standard deviation for each measurement (the error structure depending on

the frequency, but also on the modulus and phase angle of the measured impedance as well as the calibration resistance).

4. Results

4.1. Corrosion kinetics

The corrosion kinetics are displayed in Fig. 2(a), together with the results of a previous study [4]. As usual, we can see that increasing the tin content increases the corrosion rate. The first kinetic transition occurs at about 40 days for the Zy4-1.2% and 100 days for the Zy4-0.5% Sn.

Note that the weight gain at the first transition increases (linearly) with the transition time (Fig. 2(b)).

4.2. Impedance spectra

A typical set of impedance spectra are plotted in Fig. 3, both in the Bode (Fig. 3(a)) and in the Cole–Cole (Fig. 3(b)) diagrams.

On the Bode diagram, we can see that:

- At high frequency, the phase angle is low and increases with decreasing the frequency; it can be related to the presence of the electrolyte resistance which equals a few hundreds Ohms.
- At very low frequency, a decrease of the phase angle, again related to a resistance, together with a plateau for the modulus.

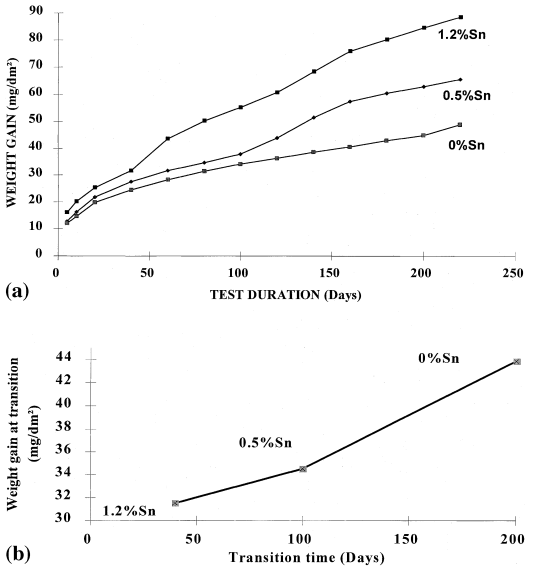

Fig. 2. (a) Corrosion kinetics of Zircaloy-4 with various tin contents. (b) Weight gain versus time at the transition for the various alloys. Data for the Zy4–0% Sn have been taken from Ref. [4].

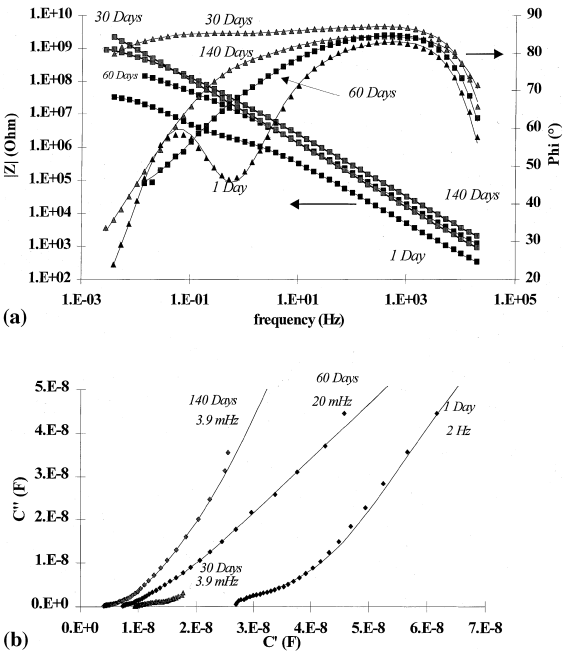

Fig. 3. Impedance spectra of Zy4–1.2% Sn corroded in 400°C steam for 1, 30, 60 and 140 days. The symbols represent the experimental points, while the continuous lines are the fitted spectra. (a) Bode diagrams. (b) Cole–Cole plots (the lowest displayed frequency are indicated besides the corresponding points).

- In between, the phase evolves between 60° and 85°, which means that the oxide film is mainly capacitive. This is confirmed by the evolution of the modulus, increasing when decreasing the frequency, the slope (in logarithmic scales) being slightly less than 1. In fact, we notice two slopes at high and low frequencies, sign of the presence of two capacities in the equivalent circuit.

On the Cole–Cole diagram, the interpretation is not straightforward, however, simulations of various electrical circuits help us to recognize the presence of two resistors and two capacities in the equivalent circuit. The details of these simulations are beyond the scope of this paper.

Note the excellent agreement between the data points and the fitted lines, on both representations. As mentioned earlier, this is the result of the choice of an adequate electrical equivalent circuit but also of a realistic error structure.

4.3. Evolution with the soaking time

Fig. 4(a) displays the evolution of the impedance spectra with the soaking time of a Zy4–0.5% Sn sample, after 30 days of corrosion. It is thus a pre-transition sample.

The extrapolation of the capacity at infinite frequency does not evolve significantly with the soaking time (Fig. 4(a)), meaning that the total thickness of the film is constant. On the contrary, the low frequency part of the diagram evolves somewhat, which can be interpreted in terms of penetration of the electrolyte in the 'porous' outer layer. In the mean time, the dispersion factor increases, leading to the same interpretation. Such an evolution is observed qualitatively for all the samples, the change being more pronounced on post-transition samples.

In Fig. 4(b), we plotted the fitted reciprocal capacitances of the different layers (total oxide layer, porous outer and dense inner layers) as a function of the soaking time. We have seen (Eq. (1)) that the reciprocal capacitances are proportional to the thicknesses, and the factor of proportionality will be determined in Section 5.1. While the total thickness is rather constant as previously deduced from the Cole–Cole diagrams, the penetrated layer thickness increases and reaches a plateau after a few days of immersion. Some dispersion parameters evolve slightly after the steady state is reached for the thicknesses, denoting some slower processes involving the electrolyte. Some studies by Cox [9,19,21] have shown that a plateau is reached only a few hours after immersion. Wikmark [17] proposes rather a few days, more in accordance with our results. Our measurements have not been performed fast and repeatedly enough to determine accurately the onset of the plateau, and thus are compatible with both authors. However, the apparent discrepancy between the two authors can be understood considering that Cox used impedance measurements at only one rather high frequency (1 kHz), where we found that the spectra do not evolve a lot, while Wikmark used whole impedance spectra down to low frequencies (10 mHz), and thus is able to detect slower processes. Garzarolli [23] indicated that the time necessary to obtain the stable state depends also greatly on the sample (it is very long just before the transition, very short after).

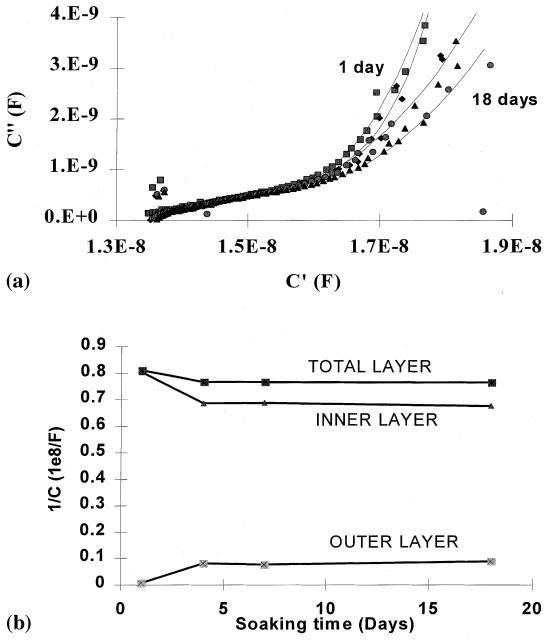

Fig. 4. Influence of the soaking time for the Zy4–0.5% Sn sample corroded for 30 days in 400°C steam. (a) Cole–Cole diagrams. The numbers written on the graphs represent the soaking time. (b) Evolution of the fitted reciprocal capacitance of the inner and the outer layer, and their sum (the total layer) with the soaking time.

We thus have seen that the penetration of the electrolyte into the pores is detectable. The oxide layer can be described as a three-layer system: the external layer immediately soaked, the intermediate one where the diffusion of the electrolyte is slow, and the inner layer being never soaked. In the following, however, we will assimilate the two first layers as the outer layer, since the intermediate zone is rather thin, and always difficult to determine accurately.

In some preliminary experiments in order to investigate the effect of the electrolyte concentration, we immersed the samples first in H_2SO_4 0.01M for a few days, then moved them to H_2SO_4 0.1M. We observed that the layer thicknesses are not influenced by the concentration change, but some other parameters of the equivalent circuit vary. Specifically, the resistance of the external layer, as well as its characteristic frequency increase by a factor of about 10, that is the ratio of the concentrations of the electrolytes. On the contrary, the inner layer resistance and characteristic frequency do not change significantly. These experiments confirm that the outer layer is penetrated by the electrolyte, and that its resistance as well as its dispersive behavior is mainly due to the effect of the electrolyte in the pores.

4.4. Evolution with the oxidation time

The evolution of the spectra with the oxidation time has been studied for the longest soaking times, when the steady state is achieved. Spectra have been displayed in Figs. 3 and 5 for the Zy4–1.2% Sn and Zy4–0.5% Sn, respectively.

For the Zy4–0.5% Sn, the Bode diagrams (Fig. 5(a)) are very similar for all the samples but the last one (140 days of oxidation) which is the only post-transition sample. Before the transition, the films look very capacitive (we get a nearly straight line with a slope equal to -1 for the modulus, while the phase angle lies about 90°). The post-transition sample presents a much more resistive behavior. On the Cole–Cole diagrams (Fig. 5(b)), the curves for the pre-transition samples remain close to the C' axis, leading again to the conclusion that the film is essentially capacitive (the dielectric or

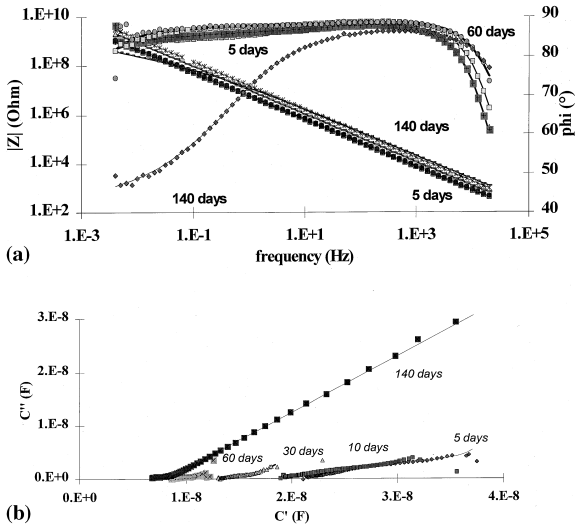

Fig. 5. Impedance spectra of Zy4–0.5% Sn corroded in 400°C steam for 5, 10, 30, 60 and 140 days. The symbols represent the experimental points, while the continuous lines are the fitted spectra: (a) Bode diagrams; (b) Cole–Cole plots.

resistive losses represented by the C'' axis are very small). This is no more the case for the post-transition sample. In addition, we can see that the capacity at infinite frequency decreases when increasing the oxidation time, i.e. the weight gain, and that the spread of the spectra on the C'-axis, even when normalized by the capacitance at infinite frequency (i.e. what we called the dispersive factor df') decreases with the oxidation time before transition, and increases drastically after.

The evolution is somewhat different for the Zy4–1.2% Sn (Fig. 3), though the same trend can be observed. At the very beginning of the oxidation (1 day), the film is very resistive, with a well-defined relaxation on the Bode diagram at about 1 Hz (Fig. 3(a)). After 30 days of oxidation, the film is mainly capacitive, like the Zy4–0.5% Sn sample before the transition. After the transition the resistive character reappears, as stated by the evolution of the phase angle and the existence of a plateau of the modulus toward the lowest frequencies. On the Cole–Cole diagrams (Fig. 3(a)), the same evolutions as for the Zy4–0.5% Sn can be noted, i.e.:

- the decrease of the capacitance at infinite frequency with the increase in the oxidation time;
- the decrease of the dispersion factor before the transition and its increase after this point.

However, for all the spectra, the C'' component of the Cole–Cole diagrams is significant, much higher than for the Zy4–0.5% Sn. The film is deduced to be more resistive (the global resistance is lower).

In Fig. 6 are presented the evolution of some fitted parameters with the oxidation time, particularly the thickness of each layer and its resistivity as well as the computed global dispersion factor (the evolution of the dispersion parameters is more complex).

We observe that:

- The thickness of the outer layer is rather constant before the transition, and increases after (Fig. 6(a) and (b)).
- The inner layer appears very thin at the early beginning of the oxidation and thickens with increasing oxidation time. After the transition, its thickness decreases somewhat for the Zy4–1.2% Sn, while it continues to increase for the Zy4–0.5% Sn. However, as we will see below, its dielectric and resistive properties change, so that the the evolution of its thickness is perhaps not the most important parameter.
- The resistivity (in fact the product of the resistance by the capacitance, i.e. the resistance divided by a factor proportional to the thickness of the layer) of the inner layer is much higher than that of the outer one; in addition, these resistivities are roughly constant or increase before the transition, and drop down after.
- The global dispersion factor decreases before the transition and increases sharply at the transition. We can interpret this fact saying that the 'compacity' of the oxide film, related to the inverse of the dispersion factor, increases and reaches a maximum at the transition, as the oxidation rate slows down. Then, the oxide 'breaks' (or becomes more porous) and the kinetic transition occurs. In addition, we can see that the dispersion factor is much lower for the low-tin zircaloy.
- The dispersion parameters of Jonscher's law evolve also markedly with the oxidation time. The characteristic frequencies (obtained by dividing the characteristic pulsation by 2π) are much higher for the outer than for the inner layer. For the outer layer, it increases slightly with the oxidation time before the transition, and more significantly after. For the inner layer, the sketch is less clear because actual dispersion parameter could not be fitted for the Zy4–0.5% Sn: the layer exhibits no dispersion in the frequency range we investigated, i.e. the characteristic frequency should be very low and/or the dispersion index very high (close to 1). To evidence a dispersion, measurements should be performed at lower frequencies (0.1 mHz or below). However, for the Zy4–1.2% Sn, it is very clear that the increase in the characteristic frequency of the inner layer is very sharp at the transition, about three orders of magnitude.

At last, the dispersion index n of the outer layer remains approximately constant (or increases slightly) during all the oxidation process. On the contrary, that of the inner layer is lower after the transition than before (again, fitted parameters are lacking before the transition for the Zy4–0.5% Sn).

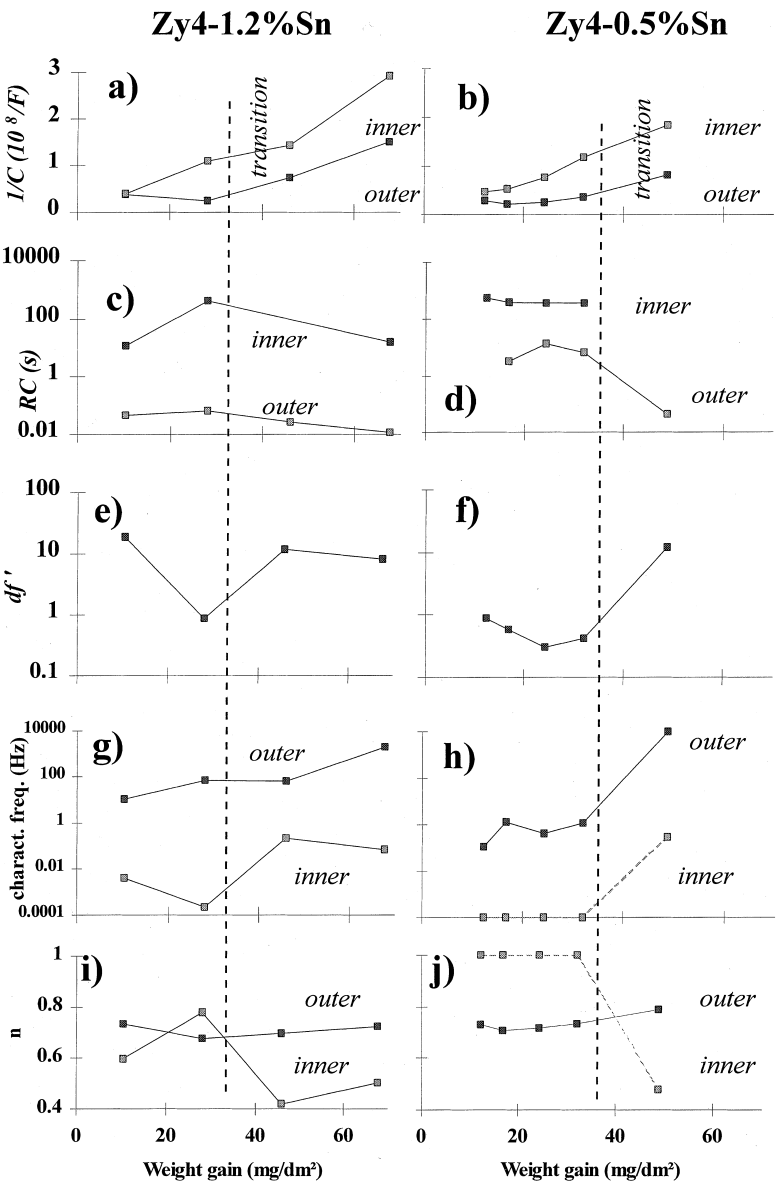

Fig. 6. Evolution with the weight gain of: (i) The fitted reciprocal capacitances of the outer and total layers (a) Zy4–1.2% Sn, (b) Zy4–0.5% Sn. In these graphs, the X-axis can be considered as the outer surface of the oxide layer, the upper curve the metal/oxide interface, and the curve in-between the separation between the two layers ox the oxide. (ii) The products of the fitted capacitance by the fitted resistance of the inner and outer layers. This parameter is related to the intrinsic resistivity of each layer. In some cases, the resistance of a layer could not be fitted, meaning that its influence on the spectra was too small to be accurately detected (it does not mean that the resistance equals zero or is very high) (c) Zy4–1.2% Sn, (d) Zy4–0.5% Sn. (iii) The global dispersion factor df′ computed from the Cole–Cole diagram (e) Zy4–1.2% Sn, (f) Zy4–0.5% Sn. (iv) The characteristic frequencies of each layer (g) Zy4–1.2% Sn, (h) Zy4–0.5% Sn (in this case the characteristic frequencies of the inner layer before the transition, below the frequency range investigated, see text, have been displayed arbitrarily at 10^{-4} Hz). (v) The dispersion indices n of each layer (i) Zy4–1.2% Sn, (j) Zy4–0.5% Sn (in this case the index of the inner layer before the transition which could not be fitted, see text, have been displayed arbitrarily at 1).

5. Discussion

We have seen in the previous section that from the beginning of the oxidation the oxide film is constituted of two layers, the outer one being porous, the inner one dense; that their thickness and properties evolve with the oxidation time, particularly at the transition, and with the tin content. The global dispersion factor increases

markedly at the transition. We will now discuss these results first to get actual thickness of each layer (i.e. to convert the reciprocal capacitances into thicknesses), then to get the implication of the bilayered structure of the oxide film, to point out the transition mechanism and the role of tin.

5.1. Correlation between the weight gain and C'_∞

The oxide layer thickness th can be evaluated either from the weight gain WG,

$$\mathrm{th} = \alpha \mathrm{WG} \tag{4}$$

with

$$\alpha \sim 1/15\ \mu\mathrm{m\ mg^{-1}\ dm^2} \tag{5}$$

or from the capacitance C' assuming relation (1). Combining Eq. (1) and Eq. (4) we obtain

$$\frac{1}{C''} = \frac{\alpha}{\varepsilon_o \varepsilon_r S} \mathrm{WG}. \tag{6}$$

In Fig. 6(a) and (b), we plotted $1/C'_\infty$ versus WG for both alloys. We can deduce from the slope the value of α/ε_r and, assuming Eq. (5), the value of ε_r. We find $\varepsilon_r = 19$ for the Zy4–1.2% Sn and $\varepsilon_r = 21$ for the Zy4–0.5% Sn. These values lay within the (wide) range of the literature data (13–22). Rosecrans [18] stated and computed that the dielectric constant of bulk zirconia is about 22, close to our values. We do not expect a big difference in the relative permittivities between bulk zirconia and oxide film. Hence, this gives some confidence in the data interpretation, specially the equivalent circuit. Moreover, some other parameters like the resistivity or the characteristic frequencies are found within or nearby the explored frequency domain (about 1 mHz to 20 kHz), which is also a proof of the reliability of the fitting.

The scatter in the data we observe from the straight line can be attributed to several factors: the accuracy of both measurements (weight gain and capacitance) but also the inhomogeneity of the oxide layer thickness (impedance measurements are performed on 1 $\mathrm{cm^2}$, weight gain on about 12 $\mathrm{cm^2}$).

5.2. Bilayered structure of the oxide film

The structure of post-transition oxide film as a bilayered material, the outer layer being cracked or 'porous', is acknowledged since a lot of years (an early review is given in Refs. [18,23]). The same structure for pre-transition oxides was proposed, but less unanimously: Cox [8] by his mercury porosimeter measurements observed no resistance drop on pre-transition films; Garzarolli [23] on uniform corrosion films stated that "the non-penetrated oxide layer is observed to be thinner than the total oxide thickness..." but that "major deviations are observed in the post-transition regime".

In this study, we evidenced by recording and fitting impedance spectra on a wide frequency range that the oxide film is structured in two layers with different properties even before the kinetic transition. In addition, the porous layer in pre-transition films represents an important part of the total thickness at the beginning of the oxidation.

The current modelization of the kinetic law generally assumes the layer to be compact before the transition, and partly porous after. Such a study has been published recently by Garcia et al. [29], deducing the thickness of the dense layer from the oxidation data and assuming a simple diffusion model. As a consequence of the previous paragraph, such a modelization should take into account only the dense layer and its evolution as a diffusion barrier. Furthermore, since the porous layer thickness is rather important during the first days of the oxidation, the kinetic should be controlled not by diffusion processes but by interfacial processes during this first period.

This bilayered structure oversimplifies the actual structure since it does not take into account the porosity gradient evidenced by the soaking experiments: as soon as the sample is immersed, two layers are seen, meaning there is a region of immediate penetration. The evolution with the soaking time up to the steady state indicates there is a gradient of porosity in the layer.

To our knowledge such a microstructure has not been observed by TEM up to now; the external equiaxed layer described by some authors (for example Pêcheur [30]) should not be matched with our external porous layer, as the thicknesses are rather different. However, the same kind of impedance studies as well as SIMS studies of hydrogen profiles through the oxide thickness performed on Zircaloy-4 specimens oxidized in 415°C steam [31] leaded to the same interpretation of the oxide layer, constituted of a porous external part where the hydrogen is highly concentrated and uniformly distributed, a gradient of porosity in the intermediate layer, and a non-porous H-depleted and H-localized internal layer.

5.3. Properties of each layer

The two layers exhibit very different properties, which are summarized below: compared to the inner layer, the outer layer presents lower resistivity, higher characteristic frequency and more stable dispersive index n. Its resistivity and characteristic frequency depend, at least partly, on the electrolyte as it has been shown by varying the H_2SO_4 concentration. We can hence interpret the difference of these parameters between the inner and the outer layer as the consequence of the presence of the electrolyte in the pores of the outer layer.

It is consistent with the fact that the electrolyte is more conducting than the oxide, at least when the pores are large enough, and with the physical meaning of a characteristic frequency: higher the frequency, lower the energy involved in the process which produces the frequency dispersion.

We have no interpretation of the difference of the dispersion indices. We can suggest that it could be related partly to the development of metal/oxide interface rugosity (geometrical factors can lead to frequency dispersion). But some more theoretical work is needed from solid physicists to know the physical meaning of this parameter (and of the characteristic frequency).

5.4. Kinetic transition

We have seen that, *before the transition*, the outer layer thickness is rather constant, as well as its characteristic frequency and its resistivity. On the contrary, the inner layer thickness increases, while for the Zy4–1.2% Sn, its resistivity and dispersive index increase, while its characteristic frequency decreases (the dispersive parameters are not available for the inner layer of the Zy4–0.5% Sn, since this layer is very 'compact', and impedance spectra should have been recorded at much lower frequencies). It means that the outer layer does not change significantly, while the 'compacity' or 'barrier character' of the (Zy4–1.2% Sn) inner layer improves. The same evolution of the inner layer thickness and resistivity has been obtained in a similar study on Zy4 [31], and reinforce our conclusions. Note that the resistivity of the inner layer of Zy4–0.5% Sn remains constant and very high before the transition. It is perhaps to be correlated with the fact this layer is very compact.

At the transition, the outer layer thickens and degrades (increase in characteristic frequency and decrease in resistivity, which can be both related to an easier penetration of the electrolyte in the layer). The inner layer thickens but also evolves considerably, with

- an abrupt change in the dispersion index which reaches the value of about 0.5,
- a decrease in the resistivity (at least for the Zy4–1.2% Sn, as observed in Ref. [31]), and
- an increase in the characteristic frequency.

These last parameters are not depending on the electrolyte concentration, and overall are very different from those of the electrolyte-soaked outer layer. Their evolution should not be related to the penetration of the electrolyte, but rather to some defects or cracks, not connected to the outer surface. But again, more need to be known about their actual physical meaning to interpret further these results.

The evolutions of the dispersion parameters are summarized through the global dispersion factor which decreases before the transition and increases sharply at this point. This parameter seems thus convenient to detect the transition.

Several hypotheses exist in the literature to explain the transition, involving tetragonal to monoclinic transformation (which could create pores and easy pathways down to the interface), relaxation of the stresses, or degradation of the dense layer due to the formation of interconnected cracks. From this study, we are not able to rank the different hypotheses, but it is clear that both the outer porous and the inner barrier layers degrade at the transition, though the related microstructural change remains unclear. Both features could contribute to a corrosion acceleration. A recent study [31] suggests that the development of cracks in itself does not lead to a corrosion acceleration: it appears when the cracks connect to the outer surface. A relaxation of stresses throughout the whole oxide layer could be compatible with our observations since both layer evolves at the transition. But the actual stress gradient, its evolution at the transition and the possible cause of its evolution are still unclear.

Furthermore, if the acceleration takes place locally at different times, then the modeling of the oxide film as two homogeneous layers should be wrong: the inner one should be represented itself by at least two RC circuits in parallel, which would rise too much parameters for fitting. The thickness and properties fitted with our equivalent circuit should be considered as 'mean' values, which could explain the rather surprising fact that the inner layer thickness does not decrease significantly at the transition.

5.5. Role of tin

Superimposing the impedance spectra of both alloys in the Cole–Cole diagram evidences the drastic difference in the dielectric dispersive properties: the dispersion of the Zy4–0.5% Sn is much lower than that of the Zy4–1.2% Sn. This result appears also on the global dispersion factor displayed in Fig. 6(e) and (f). The fitted parameters exhibits the same behavior (Fig. 6): the resistivities are higher for the Zy4–0.5% Sn, while the characteristic frequencies are lower. Hence, the oxide film appears more compact or less defected on the Zy4–0.5% Sn. This is in accordance with the slower oxidation kinetics of this alloy.

These characteristics should be related to the much higher background of the Raman spectra recorded on Zy4–1.2% Sn compared to the Zy4–0% Sn in another study [5]. It was suggested that this difference in background was due to the presence of more electronic or point defects in oxide films formed on Zy4–1.2% Sn, possibly related to non-oxidized Sn atoms close to the metal/oxide interface. Though the origin of the dielectric dispersion is not established, such defects could contribute to it, so that this hypothesis is reinforced.

Another interpretation could be found in either the difference in the tetragonal content as could be interpolated from the study by Barberis [4], or in the stresses. We have no data concerning the last point, and these hypotheses are not exclusive from the previous one.

6. Conclusion

We performed a careful analysis of EIS data on two Zircaloy-4 type alloys with different tin contents (0.5 and 1.2% Sn) corroded up to 140 days in 400°C steam. The spectra were fitted with an equivalent electrical circuit consisting of two RC circuits in series, with frequency dispersed capacitances. We have shown that:

- from the beginning of the oxidation, the oxide film is globally constituted of two layers, the outer one being porous (and soaked with the electrolyte), the inner one being dense; an intermediate but rather thin zone exists, where the soaking by the electrolyte is slow,
- before the transition, the thickness and protective character of the inner layer increase, while the outer layer does not evolve,
- at the transition, both layers (thickness and dielectric properties) evolve; particularly, the global dispersion factor increases sharply at this point, and
- the oxide film developed on the low tin alloy is much more protective than on the other one.

Acknowledgements

We would like to thank Michel Ladet from Pechiney Research Center, Voreppe, France for its help in measurements, and Hervé Del Pietro from CEZUS Research Center, Ugine, France, for its implication in fitting the spectra.

References

[1] Waterside Corrosion of zirconium alloys in nuclear power plants, IAEA-TECDOC-996, January 1998.
[2] B. Cox, J.P. Pemsler, J. Nucl. Mater. 28 (1968) 73.
[3] G.P. Sabol, S.B. Dalgaard, J. Electrochem. Soc. 122 (2) (1975) 316.
[4] P. Barberis, J. Nucl. Mater. 226 (1995) 34.
[5] P. Barberis, T. Merle-Méjean, P. Quintard, J. Nucl. Mater. 246 (1997) 232.
[6] F. Barbesino, E. Brutto, R. Di Pietro, R. Sesini, Energ. Nucl. 11 (8) (1964).
[7] C. Bataillon, S. Brunet, Electrochim. Acta 39 (3) (1994) 455.
[8] B. Cox, J. Nucl. Mater. 27 (1968) 1.
[9] B. Cox, Y.-M. Wong, J. Nucl. Mater. 218 (1995) 324.
[10] F. Garzarolli, W. jung, H. Schoenfeld, Waterside Corrosion of Zircaloy Fuel Rods, EPRI-NP-2789, December 1982.
[11] O. Gebhardt, A. Hermann, G. Bart, H. Blank, F. Garzarolli, I. Ray, ASTM-STP 1295 (1996) 218.
[12] O. Gebhardt, A. Hermann, Electrochim. Acta 41 (7/8) (1996) 1181.
[13] O. Gebhardt, J. Nucl. Mater. 203 (1993) 17.
[14] O. Gebhardt, Electrochim. Acta 38 (5) (1993) 633.
[15] H. Göhr, J. Schaller, C.-A. Schiller, Electrochim. Acta 38 (14) (1993) 1961.
[16] J.N. Wanklyn, D.R. Silvester, J. Electrochem. Soc. 105 (11) (1958) 647.
[17] G. Wikmark, P. Rudling, B. Lehtinen, B. Hutchinson, A. Oscarsson, E. Ahlberg, ASTM-STP 1295 (1996) 55.
[18] P. Rosecrans, ASTM-STP 824 (1984) 531.
[19] B. Cox, C. Wu, J. Nucl. Mater. 224 (1995) 169.
[20] B. Cox, Y. Yamaguchi, J. Nucl. Mater. 210 (1994) 303.
[21] B. Cox, Y.-M. Wong, T. Hoang, J. Nucl. Mater. 223 (1995) 202.
[22] B. Cox, C. Wu, J. Nucl. Mater. 199 (1993) 272.
[23] F. Garzarolli, H. Seidel, R. Tricot, J.P. Gros, ASTM-STP 1132 (1991) 395.
[24] H. Göhr, J. Schaller, H. Ruhmann, F. Garzarolli, ASTM-STP 1295 (1996) 181.
[25] L. Durand-Keklikian, G. Cragnolino, D.D. Macdonald, Corros. Sci. 32 (3) (1991) 361.
[26] A.K. Jonscher, J. Mater. Sci. 16 (1981) 2037.
[27] J.P. Diard, B. Le Gorrec, C. Montella, Cinétique Électrochimique, Hermann, Paris, 1996, pp. 245–248.
[28] P. Barberis, Une méthode d'ajustement des spectres d'impédance obtenus sur des films d'oxyde de zirconium. in: Actes du 9ème Forum sur les Impédances Electrochimiques, Paris, November 1995.
[29] E.A. Garcia, G. Béranger, Autoridad Regulatoria Nuclear (ARN), Argentina, PI-1/97, pp. 1–10.
[30] D. Pêcheur, J. Godlewski, Ph. Billot, J. Thomazet, ASTM STP 1295 (1996) 94.
[31] Ph. Bossis, G. Lelièvre, P. Barberis, X. Iltis, F. Lefebvre, ASTM XIIth International Meeting on Zirconium in the Nuclear Industry, Toronto, June 1998, to be published.